Insights into the MALDI Process after Matrix Deposition by Sublimation Using 3D ToF-SIMS Imaging

Sebastiaan van Nuffel, Nicolas Elie, Ethan Yang, Julius Nouet, David Touboul, Pierre Chaurand, Alain Brunelle

Insights into the MALDI Process after Matrix Deposition by Sublimation using 3D ToF-SIMS Imaging

Sebastiaan Van Nuffel[†], Nicolas Elie[†], Ethan Yang[‡], Julius Nouet[§], David Touboul[†], Pierre Chaurand[†,‡,*] & Alain Brunelle[†,*]

[†]Institut de Chimie des Substances Naturelles, CNRS UPR 2301, Univ. Paris-Sud, Université Paris-Saclay, Gif-sur-Yvette, France.
[‡]Department of Chemistry, Université de Montréal, Montréal, QC, Canada.
[§]UMR GEOPS 8148 - Géosciences Paris Sud, Université Paris-Sud / CNRS, Orsay, France.

ABSTRACT: Imaging mass spectrometry (IMS) has become a powerful tool to characterise the spatial distribution of biomolecules in thin tissue sections. In the case of matrix-assisted laser desorption ionisation (MALDI) IMS, homogeneous matrix deposition is critical to produce high quality ion images and sublimation in particular has shown to be an excellent matrix deposition method for the imaging of lipids. Matrix deposition by sublimation is, however, a completely solvent-free system, which ought to prevent the mixing of matrix and analytes thought to be necessary for successful MALDI. Using 3D time-of-flight secondary ion imaging mass spectrometry, we have studied the matrix-tissue interface in 3D with high resolution in order to understand the MALDI process of lipids after matrix deposition by sublimation. There is a strong indication that diffusion is the process by which lipids migrate from the tissue to the matrix layer. We show that triacylglycerols and phospholipids have a delayed migratory trend compared to diacylglycerols and monoacylglycerols, which is dependent on time and matrix thickness. Additional experiments show that a pure lipid's capacity to migrate into the matrix is dependent on its fluidity at room temperature. Furthermore, it is shown that cholesterol can only migrate in the presence of a (fluid) lipid and appears to fluidise lipids, which could explain its co-localisation with the diacylglycerols and monoacylglycerols in the matrix.

Introduction

Matrix-assisted laser desorption ionisation (MALDI) coupled to time-of-flight (TOF) mass spectrometric detection has become a cornerstone of proteomics ever since it was shown that the presence of a low-molecular-weight crystalline matrix with a photoabsorption maximum matched to the wavelength of the laser pulse allows the desorption and ionisation of intact proteins [1]. MALDI-TOF MS is also widely used in other 'omics' such as metabolomics [2], lipodomics [3,4,5] and glycomics [6] as well as other research fields involving macromolecules [7]. Despite the technique's profound importance, the MALDI mechanisms are not yet well understood [3,8,9]. It is known that homogeneity of the matrix-analyte mixture increases the probability to bring analyte molecules into the gas phase and to generate ions [3,10]. However, it has been suggested that it is not so much the incorporation of the analyte into the matrix crystals that matters, but the surface contact between analyte and matrix, because MALDI performance is inversely proportional to crystal size [10,11].

When MALDI imaging mass spectrometry (IMS) emerged [12,13], it became a powerful tool for investigating the spatial distribution of proteins and smaller molecules (< 1 kDa) such as lipids and metabolites within thin tissue sections. MALDI IMS has since found many applications in molecular pathology and drug delivery [14,15,16]. In the case of IMS, the tissue sections can be spray-coated or microspotted with MALDI matrix [14,17]. More recently, the MALDI matrix is sublimated onto the sample [17,18]. Sublimation of matrix onto tissue is currently the best application technique for high resolution MALDI IMS, because of the enhanced purity, the very small crystal size and deposition uniformity of the matrix [17,18]. Sublimation is an excellent matrix deposition method for the imaging of phospholipids in particular [18], but ineffective for peptide and protein imaging unless followed by a rehydration step [19]. Matrix deposition by sublimation is of course a completely solvent-free system as opposed to more conventional spray methods [18]. The analytes within the tissue section are therefore never resolubilised, which should prevent the mixing of matrix and analyte deemed necessary for MALDI [18].

To understand the MALDI process of lipids after matrix deposition by sublimation, it is necessary to study the matrix-tissue interface in 3D with high depth resolution. Time-of-flight secondary ion mass spectrometry (ToF-SIMS) is highly suited to investigate the matrix-tissue interface, because the combination of label-free molecular 2D imaging and the development of novel ion beams for

sputtering [20, 21] makes it possible to render label-free 3D chemical images with micrometric lateral resolution and nanometric depth resolution [22]. Using a Bismuth (Bi) liquid metal ion gun (LMIG) in the so-called high current bunched mode as an analysis beam, a beam spot of 1-2 µm is attained with an information depth of < 3 monolayers (≈ 1 nm) in the so-called static regime [23]. Using an argon (Ar) gas cluster ion beam (GCIB) as a sputter beam, a depth resolution of 7-10 nm can be attained [24].

Previously, Pour *et al.* [25] investigated 2,5-dihydroxybenzoic acid (DHB) sublimated onto rat brain cerebellum tissue in the context of matrix-enhanced SIMS (ME-SIMS) and observed a significant enhancement in ion yield for several lipid species. Molecular depth profiling using a C_{60}^{2+} ion beam showed an accumulation of lipid species such as phosphatidylcholine (*m/z* 184.1), cholesterol (*m/z* 369.3) and vitamin E (*m/z* 430.4) in the top analysis layers, suggesting that lipids are extracted to the sample surface by the sublimed matrix making them accessible for surface analysis using the primary ion beam [25]. The authors argue that the improvement of high mass signals is caused by the removal of excess cholesterol or by a selective lipid concentration on the surface. They also observed indications that lipid fragmentation is reduced in the presence of DHB. However, no research has been conducted so far into specifically understanding the MALDI process of lipids after matrix deposition by sublimation using ToF-SIMS imaging to study the matrix-tissue interface in 3D with high resolution.

In this article, we investigate the MALDI process of lipids after matrix deposition by sublimation using MALDI MS experiments and 3D ToF-SIMS imaging. Our samples are mouse or calf liver tissue sections prepared for MALDI imaging, *i.e.* mounted on conductive indium tin oxide (ITO) coated microscope slides and coated with a DHB matrix layer by sublimation. We successfully imaged the full thickness of our samples using ToF-SIMS with high depth resolution and observe lipid migratory patterns that elucidate the results of our MALDI MS experiments, providing important insights into the MALDI mechanisms of lipids after matrix deposition by sublimation.

Materials and Methods

Sample Preparation for MALDI MS. Three frozen mouse liver tissues were sectioned (14 µm thick) using a Leica CM3050 cryostat (Leica Microsystems GmbH, Wetzlar, Germany) and thaw-mounted on ITO-coated glass microscope slides. 2,5-DHB matrix (Sigma-Aldrich St. Louis MO, USA - 149357) was applied to the tissue by sublimation using a home-built sublimation system [17]. Either an optimal (292 ± 97 µg/cm²) or an excessive thickness (575 ± 109 µg/cm²) of matrix was sublimated (n = 5 for each thickness). The optimal thickness was decided based on maximizing the overall signal intensity in the *m/z* 500 – 900 range while keeping the laser fluency, laser spot size, shot number, etc. constant. Samples were kept in a -20°C refrigerator under a nitrogen atmosphere for prolonged storage of 1 to 7 days.

Sample Preparation for ToF-SIMS. The calf liver tissue, bought from a local butcher, was stored in a -80°C freezer. Prior to matrix deposition, the calf liver tissue was sectioned (16 µm) at -20°C using a cryostat system (Leica CM3050 S), thaw-mounted on conductive ITO-coated glass microscope slides and subsequently dehydrated in a vacuum desiccator. 2,5-DHB matrix was applied to the tissue sections by sublimation using a home-built sublimation system [17]. In total, single 3D ToF-SIMS images were acquired from ten individual samples. On average (383 ± 109) µg/cm² (n = 10) of matrix was deposited. Samples were kept in a vacuum desiccator between manipulations and, for prolonged storage, they were kept at 5°C under a nitrogen atmosphere. For the sputter rate determination of sublimated DHB, three 3D ToF-SIMS images were acquired from one sample of pure DHB on top of an ITO coated microscope slide. For the sputter rate determination of tissue, three 3D ToF-SIMS images were acquired from one sample of pure tissue on top of an ITO coated microscope slide.

In the case of the spotting experiments, cholesterol-2,3,4-$^{13}C_3$ (Sigma-Aldrich, St. Louis MO, USA - 749478), 1,2-dipalmitoyl-*sn*-glycero-3-phosphocholine and 1,2-dipalmitoleoyl-*sn*-glycero-3-phosphocholine (Avanti Polar Lipids, Alabaster AL, USA - 850355 and 850358, respectively) were first dissolved in chloroform (20 mg/mL) and subsequently a droplet of 0.5 µL was spotted on a conductive ITO-coated glass microscope slide and left to dry prior to the mounting of tissue sections and/or matrix deposition. In the cases where the cholesterol and phospholipid standards were combined, their solutions were mixed together in a 1:1 ratio and then a droplet of 0.5 µL was spotted. For all spotting experiments, single 3D ToF-SIMS images were acquired from two individual samples.

Atomic Force Microscopy. In order to measure sputter crater depths and assess the samples' surface, topographical and phase images were acquired using a Dimension 3100 setup (Bruker) operated in tapping mode and equipped with a OTESPA silicon nitride tip. The data was analysed and processed using NanoScope Analysis (Version 1.5, Bruker, USA).

White Light Interferometry. In order to measure sputter crater depths and assess the samples' surface topography, 3D topographical maps were acquired using a white light interferometer (GBS smartWLI-basic). The resulting image data was read using Kaitai Struct Compiler 0.6 and Python 3.6.1 with hdf5storage 0.1.14 and kaitaistruct 0.7 packages and subsequently exported to Matlab (Release 2016b, The MathWorks, Inc., Natick, Massachusetts, United States) for image processing and analysis.

MALDI MS. The MALDI MS measurements were performed in positive reflectron mode over a window of *m/z* 0-1500 on an ultrafleXtreme TOF/TOF mass spectrometer (Bruker Daltonics, Billerica MA, USA) with a laser energy of 60% and a global attenuator offset of 40%. Ion signals

from 25 laser shot series were acquired from single tissue coordinates. Measurements were performed immediately after matrix deposition and again after one day and seven days of storage. Data was imported into R (x 3.3.3) using readBrukerFlexData (x 1.8.5). Mass spectra were plotted using the built-in plot function in R. Yield results were plotted as non-normalised, linear-scaled heatmaps using an in-house R function based on MALDIquant and matrix heatmap plotting. Ion yield line plots were generated using an in-house R function based on MALDIquant for data export (no data treatment) into a data table. Each species was normalised to the maximum intensity for that species. Data is viewed using ggplot2 (x 2.2.1), with Loess smoothing and a span of 0.5.

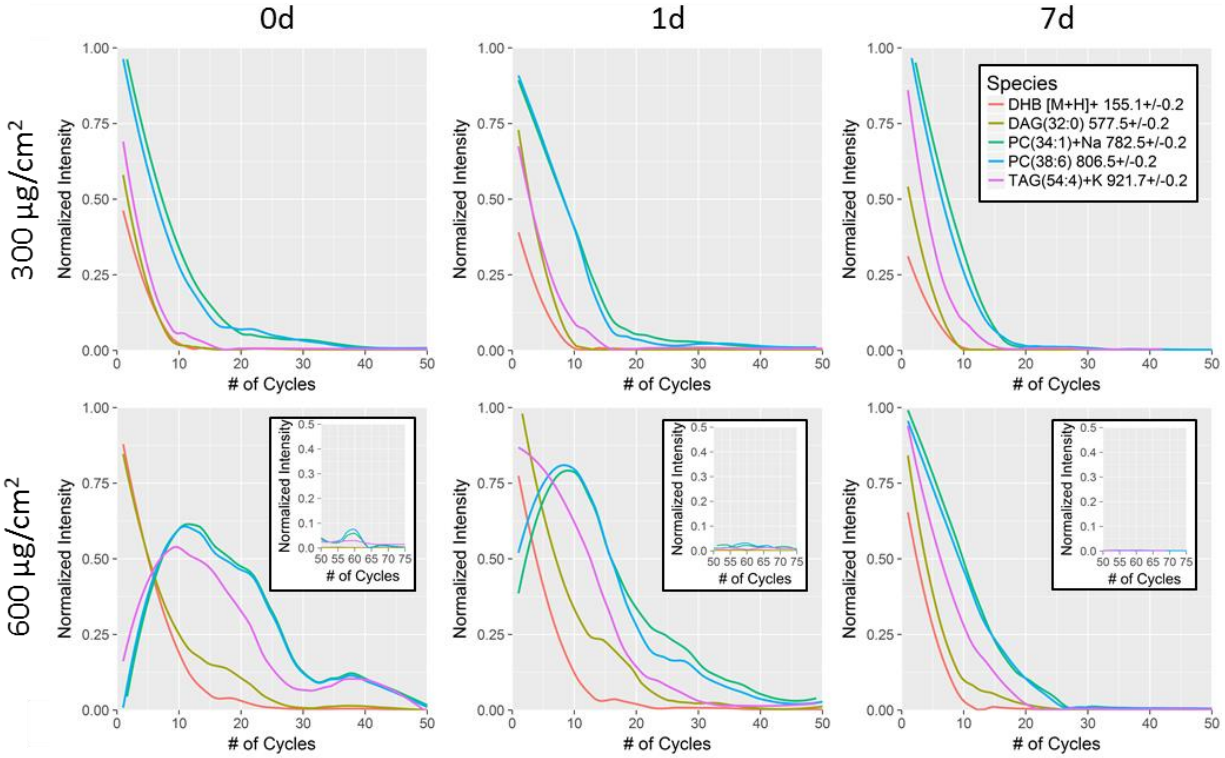

FIGURE 1. Line plots showing the normalised MALDI-MS signal intensity of five representative ion species as a function of increasing numbers of 25-shot series from a mouse liver sections for two different sublimated DHB matrix thicknesses (column) and three different wait times before analysis (row). For the excessive thickness (600 µg/cm²), preferential movement of DAG, TAG and PC to the matrix surface is clearly observed as a function of wait time. Insets show yield data for cycles 50 to 75.

ToF-SIMS. The ToF-SIMS analyses were executed using a TOF-SIMS IV instrument (ION-TOF GmbH, Münster, Germany) equipped with Bi LMIG and Ar GCIB. The primary ion beam is directed at the sample under an angle of 45° in relation to the normal and has a beam spot of 1-2 µm in the so-called high-current bunched mode. 25 keV Bi_3^+ primary ions were used in all measurements. Charging of the sample is compensated with the low-energetic 20 eV electrons of the flood gun. 20 keV Ar_{2000}^+ ion clusters were used for sputtering. Ion images were recorded in the high current bunched mode, which allows for higher mass resolution [26].

Unless stated otherwise, 200 µm × 200 µm raster scans with 128 × 128 pixels and 50 frames per scan (1 shot per pixel) were analysed. With a target current of 0.2 pA in AC mode, this resulted in an ion dose of 5.11×10^{11} primary ions per cm². 20 keV Ar_{2000}^+ clusters were used for sputtering a region of 500 µm × 500 µm between scans at a current of 3.7 nA for ten frames (14.5 s) with a cycle time of 200 µs.

For ToF-SIMS data processing, a peak search was performed to locate relevant mass peaks with a minimum of 5.0 signal-to-noise ratio (SNR) and a maximum of 0.7 background and secondary ion images were reconstructed from the raw data files with the commercial ION-TOF software (SurfaceLab 6.7). These values allowed all major peaks in the spectra to be selected and were determined empirically for these specific data sets. Images for the integrated peaks were then exported in an ASCII file format for further data processing in Matlab using in-house generated Matlab scripts [27]. The data is normalised to the total number of ion counts per pixel. Standardised (auto-scaled) PCA is performed using a training set comprising 6.1% of the total number of voxels. The information obtained using PCA allows for z-offset corrections, which are necessary for z-calibration and substrate voxel removal. All calculations were

performed on a 64-bit Windows 7 platform with 24 GB of RAM, using an Intel Core i7, 3.2 GHz processor.

Results and Discussion

MALDI MS Experiments. Positive reflectron mode MALDI-TOF MS data resulting from cycles of 25-shot series were acquired on the same tissue coordinate from mouse liver tissue sections after DHB matrix sublimation at the optimal or excessive thickness (≈ 300 or 600 µg/cm²) and measured immediately after sample preparation (t = 0d) or after storage at -20°C under nitrogen for 1 or 7 days. Mass spectra were recorded after every 25-shot series, totalling 50 cycles for the optimal thickness and 75 cycles for the excessive thickness. The spectra resulting from the first 25-shot series for all experimental conditions are shown in Supplementary Figure S1 and display large differences. All spectra, irrespective of matrix thickness and time point, show the presence of diacylglycerol ion signals in the *m/z* 500-650 range. The presence of triacylglycerol and phospholipid ion signals in the *m/z* 700-900 range varies, however. At optimal imaging matrix thickness (≈ 300 µg/cm²) ion signals for triacylglycerols and phospholipids are present in the first 25-shot series regardless of wait time. At twice the optimal matrix thickness (≈ 600 µg/cm²), at 0d, essentially only diacylglycerols are readily detected. Triacylglycerols start to be detected at 1d whereas phospholipids are clearly detected at 7d indicating preferential migration of diacylglycerols, followed by triacylglycerols and phospholipids in this order as a function of time. Supplementary Figure S2 summarises the first 50 cycles of each matrix coating condition over the *m/z* 0-1200 range as heat maps. Overall signal decay associated with increasing number of 25-shot series cycles is clearly visible. The ion intensity of five representative species (DHB $[M+H]^+$, DAG(32:0) [M+H-OH]+, PC(34:1) $[M+Na]^+$, PC(38:6) $[M+H]^+$ and TAG(52:3) $[M+K]^+$) per cycle is summarised as line plots in Figure 1. All species have been confirmed by exact mass and MS/MS (data not shown). At the optimal thickness, all species exhibited the same decay pattern, with total ablation achieved after 40 cycles. Even at this thickness, there is indication of species migration towards the matrix surface, particularly noticeable for the PC whose signals at 7d is mostly depleted after 20 cycles. The migratory behaviour is clearly demonstrated at the excessive thickness, where at 0d all but the DAG present a delayed migratory pattern, peaking around the 15th cycle and showing a broad signal distribution until the 60th cycle. After one day (1d), the TAG had preferentially migrated to the surface, as its intensity peaked within the first 5 cycles and dropped dramatically after 20 cycles, whereas the PC species both peaked soon after the 10th cycle. Another consideration is the narrowing of the TAG and PC distributions, suggesting movement towards the surface. In fact, after one week (7d), all species at the excessive thickness displayed the same decay pattern as observed at 7d for the optimal thickness, indicating their presence towards or at the matrix surface.

Given these observations suggesting preferential lipid migration to the matrix layer, the next step was to use ToF-SIMS 3D imaging of liver tissue sections prepared for MALDI IMS by sublimation to investigate the lipid distribution in the matrix layer. As a first step, it was necessary to determine the Ar_{2000}^+ sputter yield for the individual organic layers, *i.e.* liver tissue and sublimated DHB.

20 keV Ar_{2000}^+ Sputter Yield Calculation. The Ar_{2000}^+ sputter yield for the individual organic layers, *i.e.* liver tissue and sublimated DHB, was determined by preparing ITO coated slides with a tissue section or a DHB layer deposited by sublimation and sputtering 500 µm × 500 µm craters into these single layers until the inorganic substrate was reached. Because of the much lower sputter yield of inorganic material compared to organic material [28], the crater depth is a good estimate for the organic layer thicknesses. Atomic force microscopy (AFM) and white light interferometry (WLI) were used to determine the crater depth in the case of liver tissue, but only AFM was used in the case of sublimated DHB due to reflectivity issues. However, no significant difference was observed between the average tissue thickness measured by AFM and that measured by WLI (P = 0.81, two-sample t-test). The crater depth measurements also show that the thaw-mounting and dehydration step reduces the thickness of the tissue to (4.06 ± 0.34) µm (n = 3), approximately a quarter of the initial 16 µm cryostat section. Bich *et al.* [22] previously reported a reduction to 10% of the initial thickness for dried rat brain sections. AFM phase contrast images (see Supplementary Figure S3) further show that the sublimated DHB is entirely crystallised with crystal sizes around 0.5-1 µm.

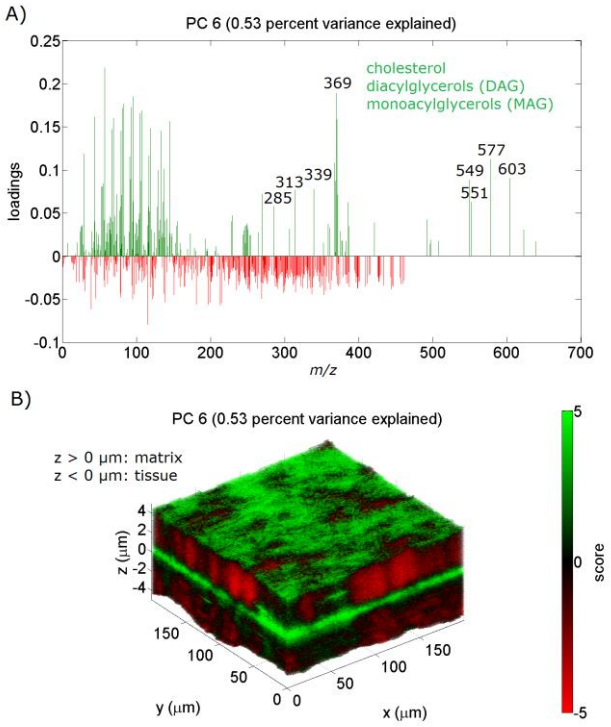

FIGURE 2. The sixth principal component (PC6) of the 3D ToF-SIMS image data of a matrix coated liver tissue section on an ITO coated microscope slide. A) The loadings plot of PC6 shows that its positive loadings contain high coefficients for the cholesterol $[M-H]^+$ ion at *m/z* 385.3 as well as its $[M+H-H_2O]^+$ fragment at *m/z* 369.3, which are positively correlated with the diacylglycerol $[M+H-OH]^+$ fragments corresponding to DAG(36:2) at *m/z* 603.5, DAG(34:1) at *m/z* 577.5, DAG(32:0) at *m/z* 551.5 and DAG(32:1) at *m/z* 549.5 and with the monoacylglycerols $[M+H-OH]^+$ fragments corresponding to MAG(18:1) at *m/z* 339.3, MAG(16:0) at *m/z* 313.3 and MAG(14:0) at *m/z* 285.2. This principal component thus pertains to the distribution of cholesterol and glycerolipids in the sample, which are co-localised. B) The 3D scores image for PC6 has had its substrate voxels removed from the data set, then undergone a z-offset correction levelling the matrix-tissue interface at z = 0 µm, and finally the z-scales of the matrix (z > 0 µm) and tissue layer (z < 0 µm) were calibrated using their respective sputter yields. Based on the 3D scores image of PC6, it is clear that the cholesterol and glycerolipid signals strongly accumulate at the surface as well as right above the matrix-tissue interface.

Finally, in order to get an accurate value for the number of sputter cycles it takes to reach the substrate, a principal component analysis (PCA) based z-offset correction was performed on the 3D ToF-SIMS images [27]. Based on three sputter craters, the ablation equals (70.6 ± 6.2) nm/cycle (n = 3) for tissue and (150.2 ± 8.9) nm/cycle (n = 3) for sublimated DHB corresponding to a 20 keV Ar_{2000}^+ sputter yield of (54.5 ± 6.1) nm^3/ion (n = 3) for tissue and (115 ± 10) nm^3/ion (n = 3) for sublimated DHB (see Supplementary Table S1).

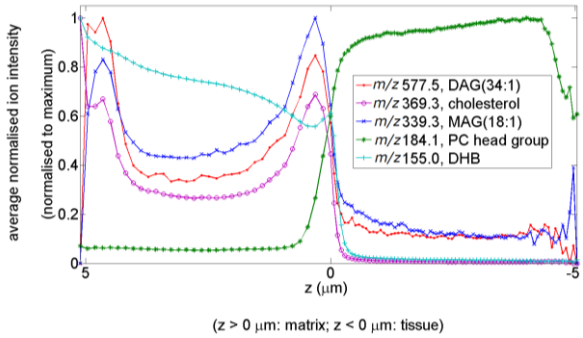

FIGURE 3. Depth profiles of the $[M+H]^+$ ion at *m/z* 155.0 as a marker ion for DHB, the $C_5H_{15}NPO_4^+$ ion at *m/z* 184.1 as a marker ion for the phosphatidylcholine head group, the $[M+H-OH]^+$ fragment of MAG(18:1) at *m/z* 339.3 as a marker ion for monoacylglycerols, the $[M+H-H_2O]^+$ fragment at *m/z* 369.3 as a marker ion for cholesterol and the $[M+H-OH]^+$ fragment of DAG(34:1) at *m/z* 577.5 as a marker ion for diacylglycerols from the ToF-SIMS image data shown in Figure 2. The matrix-tissue interface is located at z = 0 µm and the z-scales of the matrix (z > 0 µm) and tissue layer (z < 0 µm) are calibrated using their respective sputter yields.

TABLE 1. Overview of the 10 repeats of liver tissue coated with sublimated DHB matrix, indicating the wait time before being measured with ToF-SIMS, the amount of DHB deposited, the calculated matrix thickness for each 3D ToF-SIMS image and the ratio of the average normalised ion intensity in the matrix and tissue voxels for *m/z* 184.1 in each 3D ToF-SIMS image. Two-Way ANOVA shows that the main effects of both wait time (P = 0.0046) and matrix thickness (P = 0.0109) are significant. For the time factor, three levels were used namely t = 0, 1 or 7 days. For the matrix thickness factor two levels were used, defining a matrix thickness < 4 µm as 'low' and a matrix thickness > 4 µm as 'high'.

Measurement	Time in fridge (days)	DHB deposited (µg/cm²)	DHB matrix thickness (µm)	Matrix-tissue ratio of *m/z* 184.1
1	0	441	4.58 ± 0.13	0.09
2	1	308	2.57 ± 0.11	0.77
3	1	308	2.40 ± 0.10	0.70
4	0	447	5.99 ± 0.19	0.16

5	1	628	7.43 ± 0.23	0.14
6	1	326	3.29 ± 0.12	0.31
7	0	243	2.83 ± 0.14	0.28
8	7	434	4.84 ± 0.17	0.73
9	7	357	3.46 ± 0.54	1.81
10	7	338	3.11 ± 0.53	1.76

In Supplementary Figure S4, 3D scores images are shown for the principal component used for the PCA based z-offset correction. The z-axes of the scores images are calibrated using the respective sputter yields of tissue and sublimated DHB. It is also possible to calculate the 3D images surface roughness parameters, which show that DHB matrix layers generated by sublimation are very even with a total roughness R_t of 2.40 µm and a root mean square roughness R_q of 0.30 µm.

More importantly, thanks to the sputter yield calculation it is now possible to investigate the matrix-tissue interface of MALDI samples prepared by sublimation deposition with nanometric depth resolution (≈ 100 nm/scan).

Lipids in DHB Matrix. ToF-SIMS dual-beam depth profiling was performed on the full thickness of MALDI tissue samples, *i.e.* matrix layer and tissue section. PCA was first performed on the data sets. Because the first two principal components (21.53% and 11.86% variance explained, respectively) distinguish the organic material from the inorganic substrate and the DHB layer from the tissue layer respectively, it is possible to determine the tissue-substrate interface and the matrix-tissue interface and perform a PCA based z-offset correction [27] for both interfaces in the 3D scores images (see Supplementary Figure S5). Moreover, because our interest lies with the matrix and the tissue layers, we use the information from the first two principal components to first remove substrate voxels from the data set, then set the matrix-tissue interface at z = 0 µm and finally calibrate the z-scale of the matrix (z > 0 µm) and tissue layer (z < 0 µm) using their respective sputter yields, when discussing other principal components such as the particularly informative sixth principal component (0.53% variance explained) of this sample (see Figure 2). The loadings of the third and fourth principal components of this sample (3.23% and 1.55% variance explained, respectively) are very similar and differentiate the two components found in the inorganic substrate, namely ITO and glass. PC5 (0.69% variance explained) differentiates ITO from isobaric salts, *e.g.* In^+ (*m/z* 114.9) and $K_2{}^{37}Cl^+$ (*m/z* 114.9). PC3, PC4 and PC5 therefore do not yield information pertaining to our matrix and/or tissue layer. PC6, however, shows that cholesterol and glycerolipids are accumulated in the matrix layer and are co-localised. The loadings plot of PC6 (see Figure 2A) shows that the cholesterol $[M\text{-}H]^+$ ion at *m/z* 385.3 as well as its $[M+H\text{-}H_2O]^+$ fragment at *m/z* 369.3 are positively correlated with the diacylglycerol $[M+H\text{-}OH]^+$ fragments corresponding to DAG(36:2) at *m/z* 603.5, DAG(34:1) at *m/z* 577.5, DAG(32:0) at *m/z* 551.5 and DAG(32:1) at *m/z* 549.5 and with the monoacylglycerols $[M+H\text{-}OH]^+$ fragments corresponding to MAG(18:1) at *m/z* 339.3, MAG(16:0) at *m/z* 313.3 and MAG(14:0) at *m/z* 285.2 [29,30]. Based on the 3D scores image of PC6 (see Figure 2B), these signals are observed in the matrix layer. Other lipid signals that are detected in the matrix, but were not selected for PCA due to low SNR and high background, include other diacylglycerol $[M+H\text{-}OH]^+$ fragments such as DAG(36:0) at *m/z* 607.6, DAG(36:1) at *m/z* 605.5, DAG(36:3) at *m/z* 601.5, DAG(36:4) at *m/z* 599.5, DAG(34:0) at *m/z* 579.5, DAG(34:2) at *m/z* 575.5, DAG(34:3) at *m/z* 573.5, DAG(32:2) at *m/z* 547.5, DAG(30:0) at *m/z* 523.5 and DAG(30:1) at *m/z* 521.5, another monoacylglycerol $[M+H\text{-}OH]^+$ fragment at *m/z* 311.3 corresponding to MAG(16:1) and also the $[M]^{+\bullet}$ ion of vitamin E at *m/z* 430.4. The observation of these lipid ion signals is consistent with the existing literature [30] and not surprising given that the liver is a site of cholesterol synthesis and lipogenesis (fatty acid synthesis and triglyceride synthesis). No signals for triacylglycerol or glycerophosphocholine ions were detected, but that may be due to poor SNR in the *m/z* > 700 mass range.

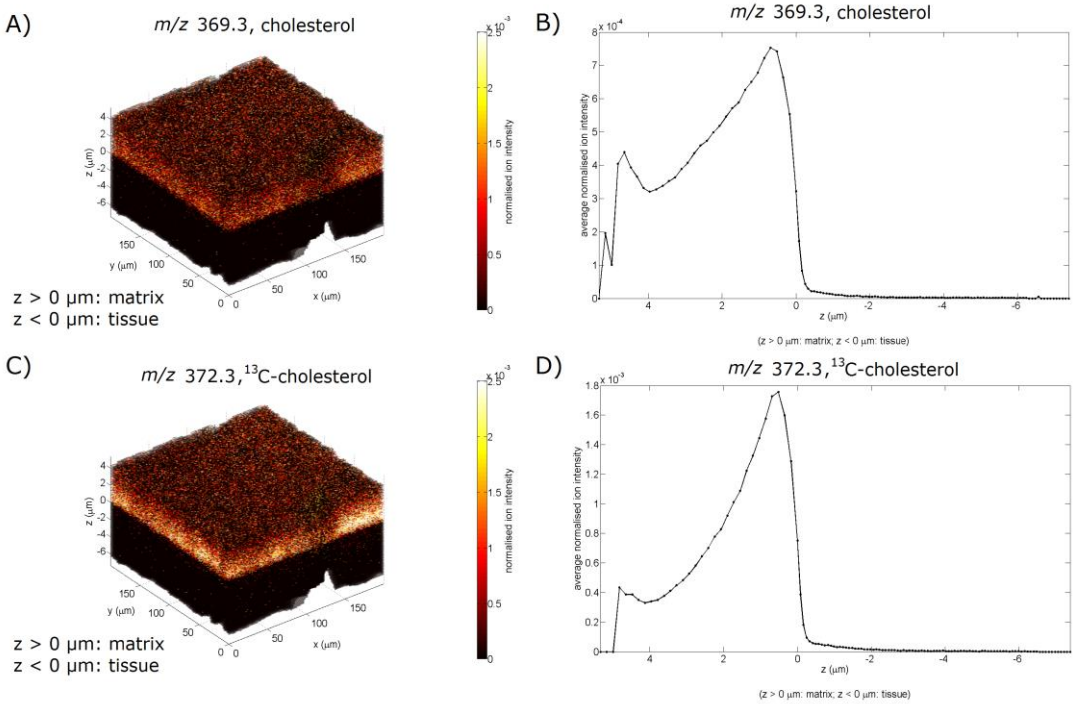

FIGURE 4. 3D ToF-SIMS image data showing the distribution of cholesterol and ^{13}C-cholesterol in a liver tissue sample coated with DHB. A) 3D Ion image for *m/z* 369.3, the $[M+H-H_2O]^+$ fragment of cholesterol. B) Depth profile of the *m/z* 369.3 ion. C) 3D Ion image for *m/z* 372.3, the $[M+H-H_2O]^+$ fragment of cholesterol-2,3,4-$^{13}C_3$. D) Depth profile of the *m/z* 372.3 ion.

Thanks to z-offset correction and z-axes calibrations, it is possible to look at the spatial distribution of individual marker ions around the matrix-tissue interface with nanometric depth resolution. From the depth profiles of *m/z* 369.3 as a marker ion for cholesterol, *m/z* 577.5 as a marker ion for diacylglycerols and *m/z* 339.3 as a marker ion for monoacylglycerols, it is clear that the cholesterol and glycerolipid ion signals are co-localised and have almost completely accumulated in the matrix with higher signals at the matrix surface and right before the matrix-tissue interface (see Figure 3). This pattern is consistent in all 10 repeats of liver tissue coated with sublimated DHB matrix.

N.B. Very similar loadings for PC1, PC2 and PC3 were obtained for all the repeats, allowing for z-offset correction and removal of the substrate voxels. Subsequent PCs differ from repeat to repeat, depending on the lipid distributions in the matrix (*vide infra*).

However, the depth profile of *m/z* 184.1 a marker ion for the phosphatidylcholine head group found in phosphatidylcholines (PC) and sphingomyelins (SM), two classes of phospholipids that are abundant in cell membranes, is different from that of the cholesterol and glycerolipid ion signals (see Figure 3) and differs between different measurements (see Supplementary Figure S6). The larger part of the intensity of the phosphatidylcholine head group ion (*m/z* 184.1) usually seems to be retained in the tissue and the intensity in the matrix appears to depend on the thickness of the DHB matrix layer as well as the waiting time before the ToF-SIMS measurement. The thinner the matrix, the higher the ratio between the average normalised *m/z* 184.1 intensity per matrix voxel and the average normalised *m/z* 184.1 intensity per tissue voxel (see Table 1). There is also a time effect as the ratio between the average normalised *m/z* 184.1 intensity per matrix voxel and the average normalised *m/z* 184.1 intensity per tissue voxel reaches a much high value after 7 days of storage. The effects of matrix thickness and time are confirmed by a two-way analysis of variance (ANOVA) and are in complete agreement with the observations made using MALDI MS. These findings indicate that for DHB, in order to successfully analyse phospholipids using MALDI IMS, samples need to be coated with a thin matrix layer of 2-4 µm corresponding to roughly 300 µg/cm². Under these conditions, nearly complete phospholipid migration to the matrix layer occurs with a fairly short turnaround time between sample sublimation and IMS analysis (typically about 15 min). A short turnaround time is preferential to minimise lipid degradation [31]. However, it has been observed that ganglioside lipid signals improve after matrix deposition by sublimation and overnight sample storage at -20°C prior to IMS analysis [32, 33]. So in some cases, applying a wait time prior to IMS analysis may be beneficial.

3D ToF-SIMS measurements of liver tissue without a DHB matrix (three replicates) similarly show that the cholesterol and glycerolipid ion signals are co-localised and concentrated in the first ten analysis layers (= 0.71 µm) of the

liver tissue sample while the intensity of the phosphatidylcholine head group ion (*m/z* 184.1) is more or less constant over the entire thickness of the sample (see Supplementary Figure S7). This is also in agreement with a number of studies that previously observed that certain ion species such as cholesterol appear to be concentrated at or just beneath the surface of tissue samples [22,34,35,36]. Sjövall *et al.* [34] showed that the cholesterol migration toward the sample surface occurs in high vacuum at temperatures higher than 0°C. In other words, the migration occurs during the freeze-drying step of the tissue section and/or *in situ* shortly after.

Correlation with the Lipid Melting Temperature. In order to get a better sense of cholesterol's capability to migrate through tissue and matrix layers, ^{13}C-labelled cholesterol (cholesterol-2,3,4-$^{13}C_3$) was spotted on an ITO coated glass slide, mounted with a liver tissue section, dehydrated and coated with sublimated DHB. The use of ^{13}C-labelled cholesterol will allow us to compare its spatial distribution with that of native cholesterol. In three-replicate 3D ToF-SIMS measurements, ^{13}C-labelled cholesterol is shown to have a very similar spatial distribution as native cholesterol (see Figure 4) and thus travelled from the bottom of the tissue into the sublimated matrix. Laterally, the ^{13}C-labelled cholesterol remained relatively localised as ^{13}C-labelled cholesterol could not be detected on the DHB surface outside of the region of the spot. In any case, this clearly demonstrates the capacity of cholesterol to migrate through about 6 µm of tissue and another 4 µm of DHB matrix, a seemingly large distance in the timespan of the sample preparation.

The liver tissue is dehydrated prior to the matrix deposition and matrix deposition by sublimation is a completely solvent-free system. The capacity of cholesterol to rapidly migrate through tissue and DHB matrix in the absence of a solvent suggests diffusion is the process by which lipids migrate from the tissue to the matrix layer. The lateral diffusion coefficient of lipids in a variety of membranes is about 1 µm²/s corresponding to an average distance travelled of about 2 µm in 1 s [37]. This fluidity is, of course, only the case when the bilayer is in the liquid crystalline phase, *i.e.* at a temperature above the lipid's melting temperature (T_m). It is therefore not unreasonable to assume that the lipids in the matrix layer have a T_m lower than room temperature to be able to diffuse to the matrix layer. The detected diacylglycerol and monoacylglycerols ion signals indicate that the glycerolipids are esters of linoleic, oleic, stearic, palmitoleic, palmitic, and myristic acid combinations. This is not particularly surprising as these are some of the most abundant fatty acids in mammalian tissue. A likely candidate for DAG(36:2) is therefore 1-stearoyl-2-linoleoyl-*sn*-glycerol with a T_m of 11.6°C and the likely candidate for DAG(36:1) is 1-stearoyl-2-oleoyl-*sn*-glycerol with a T_m of 16.4°C [38]. These T_m values support the assertion that the observed lipids in the matrix layer should have a T_m lower than room temperature. However, the likely candidate for DAG(36:0), 1,2-distearoyl-*sn*-glycerol, has a T_m of 61.6°C [38]. Although it cannot be excluded that the sample undergoes some *in situ* thermal heating due to the electron flood gun [39], it is important to note that the T_m of individual lipids not only depend on the length of the fatty acyl chains and their degree of unsaturation, but is also affected by the cholesterol content. Cholesterol is intercalated among phospholipids in the membrane and produces an intermediate state of fluidity in the lipid bilayer by decreasing the fluidity in the liquid crystalline phase and increasing the hydrocarbon chain fluidity in the gel phase, resulting in a broader phase transition [40]. Cholesterol itself, however, has a melting temperature of 148°C. This begs the question how cholesterol is able to migrate to the matrix layer.

A next set of experiments was conducted to elucidate whether cholesterol is able to migrate on its own and what effect its presence has on a lipid with low T_m and one with high T_m. To this end, spots of ^{13}C-labelled cholesterol (T_m = 148°C), 1,2-dipalmitoyl-*sn*-glycero-3-phosphocholine (16:0 PC, T_m = 41°C), 1,2-dipalmitoleoyl-*sn*-glycero-3-phosphocholine (16:1 PC, T_m = -36°C), a 16:0 PC / ^{13}C-labelled cholesterol mixture and a 16:1 PC / ^{13}C-labelled cholesterol mixture were placed on an ITO coated glass slide and coated with sublimated DHB. Cholesterol alone was not able to migrate at all, 16:0 PC also did not migrate, but 16:1 PC migrated into the DHB layer as expected (see Supplementary Figures S8 A, B and C). In the case of the mixtures, both cholesterol and the PC migrated into the matrix (see Supplementary Figures S8 D and E). These results show that cholesterol can only migrate in the presence of a (fluid) lipid and fluidises lipids with high T_m. This also explains the co-localisation of cholesterol with the detected glycerolipid signals in the matrix.

Conclusions

MALDI MS measurements indicate that triacylglycerols and phospholipids have a delayed migratory trend compared to diacylglycerols. This behaviour is amplified when twice the optimal DHB matrix thickness (≈ 600 µg/cm²) is applied. 3D ToF-SIMS imaging of liver tissue samples prepared for MALDI IMS confirmed the fast migration trend of diacylglycerols (and monoacylglycerols) to the matrix layer as well as the effects of matrix thickness and time on the migration of phospholipids to the matrix layer. These findings underpin the importance of applying the optimal amount of DHB matrix in order to successfully analyse phospholipids with a short turnaround time. It is conceivable that similar lipid migration behaviours also occur using other matrices than DHB. 3D ToF-SIMS imaging of liver tissue samples prepared for MALDI IMS further showed that cholesterol completely migrates to the matrix layer and is co-localised with the diacylglycerols and monoacylglycerol ion signals. Spotting ^{13}C-labelled cholesterol on the ITO coated glass slide before mounting the liver tissue section showed that cholesterol has the capacity to rap-

idly migrate through the entire tissue and DHB matrix layers. Because the liver tissue was dehydrated prior to the matrix deposition and since matrix deposition by sublimation is a completely solvent-free system, the distance and timespan in which this cholesterol migration occurs indicates lipids migrate *via* diffusion from the section to the matrix. Additional experiments using lipid standards showed that individual lipids need a T_m lower than room temperature to migrate into a DHB matrix layer, adding further credence to diffusion being the process by which the lipids migrate. It is also shown that cholesterol (high T_m) can only migrate in the presence of a (fluid) lipid and also appears to fluidise lipids, which explains the colocalisation of cholesterol with glycerolipids in the matrix. Based on these results, the presence of cholesterol could be considered beneficial for the MALDI imaging of lipids as cholesterol fluidises lipids with high T_m and may therefore aid their diffusion to the DHB matrix.

Although this study was focused on the migration of lipids, and more generally hydrophobic compounds, it would be very interesting in future studies, to gain insights into the possible migration of hydrophilic compounds to the matrix layer, more specifically peptides and proteins, although these classes of compounds remain barely detected with the current state-of-the-art SIMS technology.

ASSOCIATED CONTENT

Supporting Information

Supplementary figures S1-S8 and supplementary table S1.

AUTHOR INFORMATION

Corresponding Authors

Pierre Chaurand. E-mail: pierre.chaurand@umontreal.ca
Alain Brunelle. E-mail: alain.brunelle@cnrs.fr

ORCID

Nicolas Elie: 0000-0002-8733-0971
David Touboul: 0000-0003-2751-774X
Alain Brunelle: 0000-0001-6526-6481
Pierre Chaurand: 0000-0001-6821-7001

Author Contributions

S.V.N. designed the study, performed experiments and data analysis, and wrote the main manuscript. N.E. performed sample preparation and ToF-SIMS experiments. E.Y. performed all MALDI MS experiments and analysis. J.N. performed AFM measurements. D.T. assisted in experimental design and writing of the manuscript. P.C. and A.B. designed the study and wrote the main manuscript. P.C. and A.B. contributed equally.

ACKNOWLEDGEMENTS

This work was financially supported by the Idex Paris-Saclay Jean d'Alembert fellowship program (France), the Natural Sciences and Engineering Research Council of Canada (NSERC) and the Agence Nationale de la Recherche (France, grant ANR-2015-CE29-0007-01 DEFIMAGE). The authors would also like to thank François Nicolas and Stefan Kubsky (Synchrotron SOLEIL's Surface Laboratory, Saint-Aubin, France) for providing access to their white light interferometer, and Serge Della-Negra (CNRS, Université Paris-Saclay, Orsay, France) and Gérard Bolbach (CNRS, Université Pierre et Marie Curie, Paris, France) for useful discussions.

REFERENCES

[1] Karas, M.; Hillenkamp, F. *Anal. Chem.* **1988**, *60*, 2299-2301.
[2] Griffiths, W. J.; Wang, Y. *Chem. Soc. Rev.* **2009**, *38*, 1882-1896.
[3] Fuchs, B.; Süß, R.; Schiller, J. *Prog. Lipid Res.* **2010**, *49*, 450-475.
[4] Touboul D.; Brunelle A. In *Mass Spectrometry Imaging of Small Molecules*; He, L., Ed; Humana Press: New York, 2015; pp. 41-48.
[5] Cerruti, C.D;. Benabdellah, F.; Laprévote, O.; Touboul, D.; Brunelle, A. *Anal. Chem.* **2012**, 84, 2164-2171.
[6] Turnbull, J. E.; Field, R. A. *Nat. Chem. Biol.* **2007**, *3*, 74-77.
[7] Raeder, H. J. S. W.; Schrepp, W. *Acta Polym.* **1998**, *49*, 272-293.
[8] Zenobi, R.; Knochenmuss, R. Mass Spec. Rev. **1998**, 17, 337-366.
[9] Knochenmuss, R. *Analyst* **2006**, 131, 966-986.
[10] Liang, C. W.; Lee, C. H.; Lin, Y. J.; Lee, Y. T.; Ni, C. K. *J. Phys. Chem. B* **2013**, *117*, 5058-5064.
[11] Trimpin, S.; Räder, H. J.; Müllen, K. *Int. J. Mass Spectrom.* **2006**, 253, 13-21.
[12] Spengler, B.; Hubert, M.; Kauffmann, R. Proceedings of the 42nd Annual Conference on Mass Spectrometry and Allied Topics **1994**, 1041.
[13] Caprioli R.M.; Farmer T.B.; Gile J. *Anal. Chem.* **1997**, 69, 4751-4760.
[14] Cornett, D. S.; Reyzer, M. L.; Chaurand, P.; Caprioli, R. M. *Nat. Methods* **2007**, *4*, 828-833.
[15] Kadar, H.; Le Douaron, G.; Amar, M.; Ferrié, L.; Figadère, B.; Touboul, D.; Brunelle, A.; Raisman-Vozari, R. *Neurotox. Res.* **2014**, 25, 135-145.
[16] Touboul, D.; Roy, S.; Germain, D.P.; Chaminade, P.; Brunelle, A.; Laprévote, O. *Int. J. Mass Spectrom.* **2007**, 260, 158-165.
[17] Thomas, A.; Charbonneau, J. L.; Fournaise, E.; Chaurand, P. *Anal. Chem.* **2012**, 84, 2048-2054.
[18] Hankin, J. A.; Barkley, R. M.; Murphy, R. C. *J. Am. Soc. Mass Spectrom.* **2007**, *18*, 1646-1652.
[19] Yang, J.; Caprioli, R. M. *Anal. Chem* **2011**, *83*, 5728-5734.
[20] Gilmore, I.S. *J. Vac. Sci. Technol. A* **2013**, *31*, 050819.
[21] John S Fletcher, J.S.; Vickerman, J.C.; Winograd, N. *Curr. Opin. Chem. Biol.* **2011**, *15*, 733-740.
[22] Bich, C.; Havelund, R.; Moellers, R.; Touboul, D.; Kollmer, F.; Niehuis, E.; Gilmore, I.S.; Brunelle, A. *Anal. Chem.* **2013**, *85*, 7745-7752.
[23] Hagenhoff, B. *Microchim. Acta* **2000**, *132*, 259-271.
[24] Lee, J. L. S.; Ninomiya, S.; Matsuo, J.; Gilmore, I. S.; Seah, M. P.; Shard, A. G. *Anal. Chem.* **2009**, *82*, 98-105.
[25] Pour, M. D.; Malmberg, P.; Ewing, A. *Anal. Bioanal. Chem.* **2016**, *408*, 3071-3081.
[26] Sodhi, R.N.S *Analyst* **2004**, 129, 483-487.
[27] Van Nuffel, S.; Parmenter, C.; Scurr, D. J.; Russell, N. A.; Zelzer, M. *Analyst* **2016**, 141, 90-95.
[28] Cumpson, P. J.; Portoles, J. F.; Barlow, A. J.; Sano, N.; Birch, M. *Surf. Interface Anal.* **2013**, *45*, 1859-1868.
[29] Passarelli, M. K.; Winograd, N. *BBA-Mol. Cell Biol. L.* **2011**, *1811*, 976-990.
[30] Debois, D.; Bralet, M. P.; Le Naour, F.; Brunelle, A.; La-prévote, O. *Anal. Chem.* **2009**, *81*, 2823-2831.

[31] Patterson N.H.; Thomas A.; Chaurand P. *J. Mass Spectrom.* **2014**, *49*, 622-627.
[32] Weishaupt, N.; Caughlin, S.; Yeung, K.K.; Whitehead, S.N. *Front. Neuroanat.* **2015**, *9*, 155.
[33] Yang, E.; Dufresne, M.; Chaurand, P. *Int. J. Mass Spectrom.* **2017**, DOI: 10.1016/j.ijms.2017.09.011.
[34] Sjövall, P.; Johansson, B.; Lausmaa, J. *Appl. Surf. Sci.* **2006**, *252*, 6966-6974.
[35] Debois, D.; Brunelle, A.; Laprévote, O. *Int. J. Mass Spectrom.* **2007**, 260, 115-120.
[36] Jones, E. A.; Lockyer, N. P.; Vickerman, J. C. *Anal. Chem.* **2008**, *80*, 2125-2132.
[37] Berg J.M.; Tymoczko J.L.; Stryer L. Biochemistry, 5th ed.; WH Freeman: New York, 2002.
[38] Di, L.; Small, D. M. *Biochemistry* **1995**, 34, 16672-16677.
[39] Gilmore, I.S.; Seah, M.P. *Appl. Surf. Sci.* **2002**, *187*, 89-100.
[40] Bhattacharya, S.; Haldar, S. *BBA-Rev Biomembranes* **2000**, *1467*, 39-53.